Artifact removal in magnetoencephalogram background activity with independent component analysis

Artifact Removal in Magnetoencephalogram Background Activity with Independent Component Analysis

Javier Escudero*, *Student Member, IEEE*, Roberto Hornero, *Member, IEEE*, Daniel Abásolo, *Member, IEEE*, Alberto Fernández, and Miguel López, *Member, IEEE*

***Abstract*—The aim of this study was to assess whether independent component analysis (ICA) could be valuable to remove power line noise, cardiac, and ocular artifacts from magnetoencephalogram (MEG) background activity. The MEGs were recorded from 11 subjects with a 148-channel whole-head magnetometer. We used a statistical criterion to estimate the number of independent components. Then, a robust ICA algorithm decomposed the MEG epochs and several methods were applied to detect those artifacts. The whole process had been previously tested on synthetic data. We found that the line noise components could be easily detected by their frequency spectrum. In addition, the ocular artifacts could be identified by their frequency characteristics and scalp topography. Moreover, the cardiac artifact was better recognized by its skewness value than by its kurtosis one. Finally, the MEG signals were compared before and after artifact rejection to evaluate our method.**

***Index Terms*—Artifact rejection, higher-order statistics, independent component analysis, magnetoencephalography.**

I. Introduction

MAGNETOENCEPHALOGRAM (MEG) captures the neural activity with high spatial resolution by measuring the brain magnetic fields. This technique is not invasive, and it does not depend on any reference point [1]. Moreover, magnetic fields are less distorted than electric ones by the skull and the scalp [1]. However, MEG data must be recorded in magnetically shielded rooms with superconducting quantum interference devices (SQUIDs) to reduce external noise [1].

Unfortunately, external noise is not the only undesired signal in MEG data. In these recordings, non-cerebral sources (i.e., artifacts) always appear mixed with brain signals. The artifacts could bias the analyses, since their power may be larger than that of the brain sources [2]. For instance, the cardiac artifact is usually noticeable in MEG data [3]. Ocular artifacts can also be visible in these signals [4]. Although they can be partially controlled by the subject in short data epochs, these artifacts are likelier to appear in long recordings or when the MEG is recorded from non-collaborative subjects. In addition to these artifacts, MEG data may have strong power line noise [1]. Finally, some authors have claimed that any inner source without time structure should be removed, since it provides no information about the brain activity [5].

Several methods have been used to remove artifacts from electroencephalogram (EEG) and MEG data: epoch rejection, regression techniques [6], principal component analysis (PCA) [7] or independent component analysis (ICA) [8], [9]. The simplest method to avoid artifacts in these data is epoch rejection, which discards raw data epochs highly contaminated by artifacts. However, it may produce significant data loss [10], [11]. On the other hand, electrooculogram (EOG) regression [6] is a relatively simple way to remove ocular artifacts by projecting the EOG to the EEG channels. However, this method might produce new unexpected artifacts in the data [10]. Moreover, this technique needs to record the EOG and brain data simultaneously. In contrast, PCA can be applied to reject any kind of artifact without reference signals. This technique finds orthogonal directions of greatest variance in data [12]. Thus, PCA components are uncorrelated but not necessarily independent. Unfortunately, PCA can detach artifacts from brain signals completely only when they are orthogonal to each other, their amplitudes are dissimilar, and the additive noise power is low enough [5], [11].

ICA, a method to achieve a blind source separation (BSS) [13], has been used recently in the artifact rejection problem [5], [10], [11], [14]–[16]. ICA needs neither previous information nor orthogonality between artifacts and brain signals. Furthermore, the assumptions made about the data by ICA seem to be suitable for MEG recordings [2], [10].

A major problem in this artifact rejection method is the artifact recognition. A few studies have proposed metrics to mark several artifacts, in order to make this process easier and faster for medical doctors. Kurtosis and entropy were used to identify artifacts in EEG recordings [17]. With the addition of a correlation metric to these statistics, a method to detect

Manuscript received May 31, 2006; revised January 10, 2007. This work was partially supported by "Ministerio de Educación y Ciencia" and FEDER grant MTM 2005-08519-C02-01 and by the grant project VA108A06 from "Consejería de Educación de la Junta de Castilla y León." *Asterisk indicates corresponding author.*

*J. Escudero is with the E.T.S. Ingenieros de Telecomunicación, University of Valladolid, Spain, Camino del Cementerio s/n, 47011, Valladolid, Spain (e-mail: javier.escudero@ieee.org).

R. Hornero, D. Abásolo, and M. López are with the E.T.S. Ingenieros de Telecomunicación, University of Valladolid, 47011, Valladolid, Spain.

A. Fernández is with the Centro de Magnetoencefalografía Dr. Pérez-Modrego, Complutense University of Madrid, 28040, Madrid, Spain.

various artifacts in MEG background data was developed [18]. Other approaches have been suggested. For instance, the independent components (ICs) can be sorted depending on their time structure [5] or a reference can be used to constraint the artifact extraction [19]. An extensive study about ocular artifact rejection in EEG using EOG reference channels was performed in [20], and the scalp topography was used to remove eye blink artifacts from EEG data [21]. Moreover, another open issue is how to select the number of ICs, since few statistical criteria have been used to estimate this parameter [22], [23].

In this paper, we applied a robust preprocessing to estimate the number of ICs that composed the data. Then, a robust ICA algorithm decomposed the MEG recordings. Afterward, several criteria were proposed to detect power line noise, cardiac, and ocular artifacts. The whole process had been tested on simulated data. We wanted to test if this method could remove these artifacts from MEG background activity.

II. Methods and Signals

A. Linear mixing model and ICA algorithm

ICA may be useful in the artifact rejection problem, since it decomposes the data into ICs. These ICs can be inspected to find which are responsible for the artifacts [14], [16], [18]. The marked artifactual ICs can be removed to rebuild the signals without them. The n MEG channels, $\mathbf{x}(t) = [x_1(t), \ldots, x_n(t)]^{\mathrm{T}}$, are considered a linear mixture of m ICs, $\mathbf{s}(t) = [s_1(t), \ldots, s_m(t)]^{\mathrm{T}}$ [8], [9]:

$$\mathbf{x}(t) = \mathbf{A}\mathbf{s}(t), \tag{1}$$

where $m \leq n$ and $\mathbf{A}$ is a full rank $n \times m$ mixing matrix. This simplified model can be suitable if additive sensor noise is low enough [2]. However, a more realistic model may be used to consider external noise, which is modeled as an n-dimensional vector of additive spatially uncorrelated Gaussian noise, $\mathbf{v}(t)$ [5], [16], [18]. Thus, the model becomes:

$$\mathbf{x}(t) = \mathbf{A}\mathbf{s}(t) + \mathbf{v}(t), \tag{2}$$

where $\mathbf{s}(t)$, $\mathbf{x}(t)$, and $\mathbf{v}(t)$ have zero mean [8], [18].

In the BSS problem, only the observations, $\mathbf{x}(t)$, are available. Thus, $\mathbf{A}$, $\mathbf{s}(t)$, and $\mathbf{\Psi} = \mathrm{E}\{\mathbf{v}(t)\mathbf{v}(t)^{\mathrm{T}}\}$, where $\mathrm{E}\{\cdot\}$ is the expectation value, have to be estimated blindly from $\mathbf{x}(t)$. Several assumptions are needed to find $\mathbf{A}$ and $\mathbf{s}(t)$ using ICA [9]: independent and non-Gaussian ICs, instantaneous linear mixing, and stationary data. These assumptions have been validated for EEG and MEG data in several papers (e.g., [2], [24]). Under such assumptions, the ICs can be estimated by:

$$\mathbf{y}(t) = \mathbf{W}\mathbf{x}(t) = \mathbf{W}[\mathbf{A}\mathbf{s}(t) + \mathbf{v}(t)] = \hat{\mathbf{s}}(t) + \mathbf{W}\mathbf{v}(t), \tag{3}$$

where $\mathbf{y}(t) = [y_1(t), \ldots, y_m(t)]^{\mathrm{T}}$ is an m-dimensional vector that estimates the ICs, and $\mathbf{W} = \hat{\mathbf{A}}^{+}$ is a separation matrix (apexes "+" and "^" denote a pseudoinverse matrix and an estimated variable, respectively).

Since we have modeled the MEG data as a noisy mixture of ICs, the ICA algorithm must be robust to external noise. We have used the Cumulant-based Iterative Inversion (CII) algorithm [25]. This algorithm is robust in the sense that, although the data could be contaminated by external Gaussian noise, the estimated decomposition is asymptotically unbiased when calculations are carried out with enough samples (typically ≥ 5000) [18]. Moreover, its convergence is isotropic and independent of the source distribution [25].

B. Robust preprocessing

Before the CII algorithm was applied, we preprocessed the data to reduce the problem dimensionality and to estimate m. This preprocessing had also to be robust to external noise.

It can be useful to apply a dimensionality reduction before ICA. Firstly, when high-density recording equipment is used, the number of macroscopic inner components may be less than the number of available channels for analysis [2], [22]. Secondly, a dimensionality reduction can sometimes be needed to avoid overfitting [10], which can lead to the extraction of meaningless ICs [2]. This is due to the fact that overfitting may occur if a too high value is assigned to m [2], [9]. Finally, the dimensionality reduction helps to reduce the importance of the outer noise [22].

Usually, the preprocessing is performed by standard PCA [2], [10]. However, this approach has some drawbacks. First of all, m is frequently determined by setting a power threshold on the eigenvalue spectrum of the data covariance matrix [2], [16]. However, this criterion involves some arbitrariness. Moreover, it assumes that $\mathbf{\Psi}$ is close to zero, something that may not be true in un-averaged MEG data [23]. To overcome this problem, the eigenvalue spectrum may be split into a signal and a noise subspaces by a power threshold. Then, the external noise power is estimated from the noise subspace, and it is subtracted from the signal subspace [16], [18]. However, this method assumes that all MEG channels have the same noise power, and it retains the aforementioned subjectivity.

In contrast to those techniques, we used the preprocessing with noise reduction proposed in [23]: the unweighted least squares method of factor analysis (FA) [12]. This method takes into account the diagonal elements in $\mathbf{\Psi}$.

Let $\hat{\mathbf{A}}_{\mathrm{Pr}}$ be the estimated preprocessing mixing matrix that relates the preprocessed data, $\mathbf{z}(t)$, to $\mathbf{x}(t)$:

$$\mathbf{x}(t) = \hat{\mathbf{A}}_{\mathrm{Pr}}\mathbf{z}(t) + \mathbf{v}(t), \tag{4}$$

and define $\mathbf{C} = \mathrm{E}\{\mathbf{x}(t)\mathbf{x}(t)^{\mathrm{T}}\}$. $\hat{\mathbf{A}}_{\mathrm{Pr}}$ is iteratively computed from the eigenvalue decomposition of $(\mathbf{C} - \hat{\mathbf{\Psi}})$, and $\hat{\mathbf{\Psi}}$ is also iteratively estimated as the diagonal elements of $(\mathbf{C} - \mathbf{A}_{\mathrm{Pr}}\mathbf{A}_{\mathrm{Pr}}^{\mathrm{T}})$. The full process is detailed in [23].

Once $\hat{\mathbf{\Psi}}$ and $\hat{\mathbf{A}}_{\mathrm{Pr}}$ had reached stable values, we calculated

the prewhitening matrix, $\mathbf{Q}$, as the pseudoinverse of $\hat{\mathbf{A}}_{\mathrm{Pr}}$. Since pseudoinverse matrixes are not unique, we used [22], [23]:

$$\mathbf{Q} = \left(\hat{\mathbf{A}}_{\mathrm{Pr}}^{\mathrm{T}} \hat{\boldsymbol{\Psi}}^{-1} \hat{\mathbf{A}}_{\mathrm{Pr}}\right)^{-1} \hat{\mathbf{A}}_{\mathrm{Pr}}^{\mathrm{T}} \hat{\boldsymbol{\Psi}}^{-1}, \tag{5}$$

which considers $\hat{\boldsymbol{\Psi}}$.

Using $\mathbf{Q}$, the preprocessed data are obtained by $\hat{\mathbf{z}}(t) = \mathbf{Q}\mathbf{x}(t)$. This method assumes that m is known. However, m must also be estimated blindly from the data. Considering $m \leq n$ and the number of free parameters, a bound for the integer m can be found ($m_{\max}$) [22], [23]. In order to determine m, we used a method derived from FA based on statistical model selection with information criteria. We estimated $\hat{\boldsymbol{\Psi}}$ and $\hat{\mathbf{A}}_{\mathrm{Pr}}$ for each $1 \leq m \leq m_{\max}$. Then, the minimum description length (*MDL*) was computed for each m value as follows [22]:

$$\begin{aligned} MDL = {} & \frac{1}{2}\mathrm{tr}\left[\mathbf{C}\left(\hat{\boldsymbol{\Psi}} + \hat{\mathbf{A}}_{\mathrm{pr}}\hat{\mathbf{A}}_{\mathrm{pr}}^{\mathrm{T}}\right)^{-1}\right] + \frac{1}{2}\log\left[\det\left(\hat{\boldsymbol{\Psi}} + \hat{\mathbf{A}}_{\mathrm{pr}}\hat{\mathbf{A}}_{\mathrm{pr}}^{\mathrm{T}}\right)\right]\ldots \\ & + \frac{n}{2}\log(2\pi) + \frac{\log N}{N}\left[n(m+1) - \frac{m(m-1)}{2}\right], \end{aligned} \tag{6}$$

where N is the number of signal samples, and $\mathrm{tr}(\cdot)$ denotes the trace of a matrix. Finally, the data were preprocessed with the set of m and $\mathbf{Q}$ that minimizes the *MDL*.

C. Artifact detection metrics

In this section, we present the metrics used to detect the considered artifacts.

1) Kurtosis and skewness to detect cardiac artifacts

Let $m_n = \mathrm{E}\left\{\left(x - \mathrm{E}\{x\}\right)^n\right\}$ be the n-th central moment of an amplitude distribution. Kurtosis excess (*KrE*) and skewness (*Skw*) are defined as:

$$KrE \equiv \frac{m_4}{(m_2)^2} - 3, \tag{7}$$

$$Skw \equiv \frac{m_3}{(m_2)^{3/2}}. \tag{8}$$

KrE is negative for platykurtic amplitude distributions ("flatter" than the Gaussian one). However, if the samples are highly gathered round the distribution central values, *KrE* is positive (leptokurtic distribution) [17], [18]. In contrast, *Skw* measures the asymmetry degree of a distribution. Only if the distribution is symmetrical, *Skw* is zero. Thus, large *KrE* values and $\mathrm{abs}(Skw)$, where $\mathrm{abs}(\cdot)$ denotes absolute value, are associated with leptokurtic and asymmetric ICs, which may be due to the cardiac artifact [18].

2) Ocular artifacts detection based on spectral and scalp field features

The energy of the ocular artifacts is focused on lower frequencies than in brain or cardiac signals [20]. In addition, their power is mainly gathered near the eyes [21]. Hence, the low frequency content of the ocular artifacts and their scalp distribution have already been used to help in the detection of these artifacts in EEG [20], [21]. This suggests that these criteria may be useful to reject ocular artifacts. Thus, we compute the fraction of the power spectral density (PSD) that each IC has from 0.5 Hz to 2.5 Hz (P_{LF}). To decide whether an IC may be an ocular artifact, we set a threshold, th_{LF}, and we mark that IC as a possible ocular artifact if $P_{LF} > th_{LF}$. In order to assure that the ICs marked by P_{LF} are real ocular artifacts, we compute the IC power fraction located on the 13 frontal peripheral channels nearer to the eyes (P_{EYES}). Only if an IC has been marked by P_{LF}, and it has a P_{EYES} value larger than a threshold, th_{EYES}, it is considered an ocular artifact.

We use a receiver operating characteristic (ROC) analysis [26] with a leave-one-out cross-validation procedure to find the thresholds th_{LF} and th_{EYES}. We define the sensitivity as the rate of ocular artifacts correctly classified (true positive rate), whereas the specificity represents the fraction of non-ocular ICs properly recognized (the true negative rate). The accuracy is defined as the total number of ICs precisely classified. Finally, we set the optimum threshold as the point that provides the highest accuracy.

3) Frequency recognition of the power line interference

If an IC could isolate line noise, its spectrum would be centered at the power line frequency (50 Hz). Hence, we calculate a spectral metric, $P_{50\mathrm{Hz}}$, which measures the fraction of the PSD contained from 49.5 Hz to 50.5 Hz for each IC. Large values of $P_{50\mathrm{Hz}}$ are due to ICs that have most of their energy round 50 Hz. Thus, we set a threshold, $th_{50\mathrm{Hz}}$. The ICs are marked as line noise if $P_{50\mathrm{Hz}} > th_{50\mathrm{Hz}}$.

D. Simulated data

We used simulated data to check our method [5], [18]. These data were composed by 11 sources. Four of them (S1 to S4) were considered artifactual components, whereas the other seven (S5 to S11) simulated useful signals. These signals had the same sample frequency (169.549 Hz) and length (50 s) as the real MEG epochs described in the following subsection.

Fig. 1 depicts one example of each synthetic source. Their time plot and normalized PSD are shown. S1 corresponded to a real electrocardiogram (ECG) signal. S2 was an inner white Gaussian noise source. S3 was a real EOG, and S4 simulated power line noise (a sine wave at 50 Hz). S5 was a real MEG epoch recorded at a central position of the head. It was selected to have minimal ocular and cardiac activity. The power line noise was reduced using a Q-notch digital filter. Moreover, in order to remove any possible remainder of cardiac activity, the projection of a simultaneous ECG signal onto the MEG epoch was computed. Then, this projection was removed from S5. S6 was a 1/f noise source. Similarly to the EOG, this noise has most of its power in low frequencies. Likewise the ECG, S7 was a skewed and leptokurtic source. It was a white exponential noise source with $\lambda = 1$. Finally, S8 to S11 represented rhythmic activity. Their main frequencies were 7 Hz, 14 Hz, 21 Hz, and 28 Hz, respectively, and their

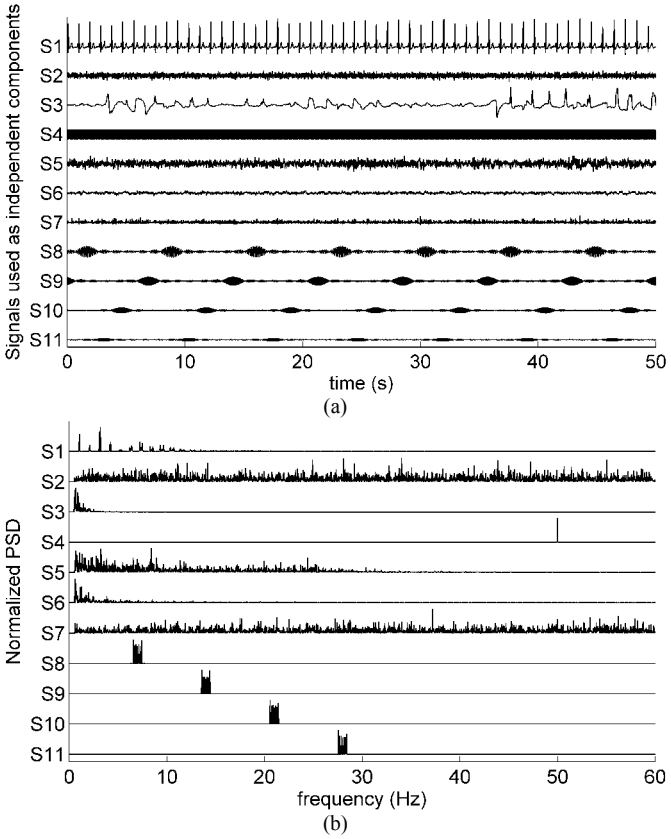

Fig. 1. Examples of synthetic sources. S1 to S4 simulated undesired signals (S1: cardiac artifact; S2: inner white Gaussian noise; S3: ocular artifact; S4: line noise). S5 to S11 simulated "useful" signals (S5: real MEG signal with minimal artifactual activity; S6: 1/f noise; S7: inner white exponential noise; S8 to S11: rhythmic signals centered at 7 Hz, 14 Hz, 21 Hz, and 28 Hz, respectively). (a) Time plot. (b) Normalized PSD.

bandwidth was 1 Hz. From these 11 source components, 52 mixed signals were created using random mixing matrixes (similarly to [18]) generated by a random Gaussian process with zero mean and standard deviation (SD) equal to one.

If the simulated artifacts (S1 to S4) and the useful sources (S5 to S11) were considered inner noise and useful signal, respectively, the inner signal-to-noise ratio (SNR) was about −5.5 dB. Moreover, additive Gaussian noise was added to every mixed signal. The additive noise power was varied, and the source delay was changed in every data set. Finally, all the mixtures were filtered using the same band-pass filter applied to the real MEG data.

E. MEG data

MEG recordings were obtained from 11 elderly subjects, who gave their informed consent for the participation in this study, which was approved by the local ethics committee.

The subjects had no past or present neurological disorders, and their average age was 68.36 ± 8.32 years (mean ± SD). The participants were asked to stay awake with eyes closed and to reduce eye and head movements while they lay on a patient bed to record the MEG. These conditions are similar to the recording protocol used in diagnostic studies. For each subject, five minutes of MEG recording were acquired with a 148-channel whole-head magnetometer (MAGNES 2500 WH, 4D Neuroimaging) in a magnetically shielded room. The MEG was registered at a sampling frequency of 678.17 Hz, and it was down-sampled to 169.549 Hz (50,863 samples). Every 5-min recording was split into 6 epochs of 50 s (8,477 samples). Thus, 66 MEG epochs were copied for off-line analysis. All epochs had cardiac artifacts, and some of them also showed ocular and/or power line ones. The epochs were digitally filtered between 0.5 Hz and 60 Hz.

III. RESULTS

We applied the proposed methodology to synthetic and real MEG data. The simulated data were used to check the validity of our method and to verify that the artifacts could be suitably identified. However, the definite assessment of the artifact rejection depends only on its performance on real MEG data.

A. Simulated data

We created 500 different synthetic data sets with mean channel SNR values (the average SNR values between mixed signals and outer noise) ranging from –9.3 dB to 16.6 dB. To assess the error in the estimation of the external noise power and the number of ICs, we preprocessed every data set ten times with the methods given in [22], [23].

Let $\boldsymbol{\Psi}$ be the actual covariance matrix of the outer noise added to the synthetic mixtures, and $\hat{\boldsymbol{\Psi}}$ be the estimation of $\boldsymbol{\Psi}$ provided by the preprocessing. The normalized error in the estimation of the external noise power (E_{norm}) was given by:

$$E_{norm} = \frac{\sum \mathrm{abs}\left[\mathrm{tr}\left(\hat{\boldsymbol{\Psi}}\right) - \mathrm{tr}\left(\boldsymbol{\Psi}\right)\right]}{\sum \mathrm{tr}\left(\boldsymbol{\Psi}\right)}. \quad (9)$$

Fig. 2(a) shows the average E_{norm} values when m took the values provided by the *MDL* metric [22]. This error was usually lower than 3.5%. Moreover, we also evaluated the performance of several methods to estimate the number of ICs (m). These methods were:

1) The *MDL* metric [22], which is denoted by "MDL."
2) To estimate m at the number of eigenvalues needed to account for a fixed fraction of the total observed variance [2], [16]. We set this fraction to 95% ("cumulative 95%") and 99% ("cumulative 99%").
3) To consider only the components which individually provided more than 1% of the total variance [2]. This approach was referred as "larger than 1%."

The m values estimated by every method are depicted in Fig. 2(b). The cumulative variance criteria overestimated m clearly, something that could produce overfitting, leading to extract distorted ICs [2], [9]. For average channel SNR values larger than 3 dB, the *MDL* estimated m accurately. For these SNR values, the "larger than 1%" metric failed slightly, as it assumed that the number of ICs was 9 or 10. For mean SNR values lower than 3 dB, the *MDL* metric underestimated m. This could cause that some real sources would be mixed into one or more extracted components. In contrast, when the mean

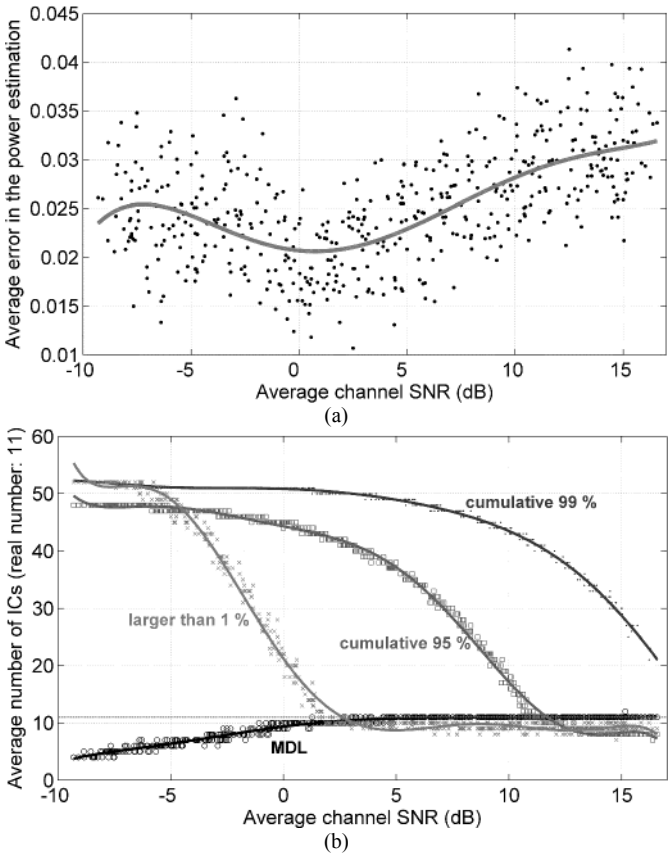

Fig. 2. Preprocessing results for synthetic data. (a) Average E_{norm} against mean channel SNR. The error was usually below 3.5%. (b) Average estimated number of ICs against mean channel SNR for several criteria: the *MDL* metric, the cumulative 95% and 99% criteria, and the "larger than 1%" approach. The *MDL* metric provides a more accurate estimation for a broader range of average channel SNR values.

channel SNR values were below 3 dB, the "larger than 1%" metric overestimated *m* similarly to the cumulative criteria.

Afterward, 20 synthetic data sets were preprocessed and decomposed by the CII algorithm [25]. For these data sets, the mean channel SNR was 7.32 ± 2.96 dB (mean ± SD). The CII algorithm did not converge in two of the 20 cases. In 15 of the 18 decomposed data sets, the cardiac, ocular, and power line artifacts were fully isolated into different ICs. In the three remaining cases, the ICs could not be completely separated, especially the cardiac artifact.

In all data sets, the line noise IC had $P_{50\text{Hz}} \geq 0.5038$, while the maximum $P_{50\text{Hz}}$ value for any other IC was 0.1526. Likewise, all ocular ICs provided $P_{LF} \geq 0.4141$, whereas the maximum P_{LF} value for any non-ocular IC was 0.2478. Thus, the detection of these artifacts was completely satisfactory, since the $P_{50\text{Hz}}$ and P_{LF} values for the corresponding artifactual ICs could be clearly differentiated from the values of any other IC. Finally, the $\text{abs}(Skw)$ and *KrE* metrics were able to detect 15 of the 18 cardiac artifacts. Both metrics failed when the cardiac artifact was mixed with other sources.

B. Real MEG data

Sixty-six MEG epochs of 50 s with several artifacts were selected for analysis. The CII algorithm [25] was applied to the MEG epochs with the step-size parameter set to 0.9 and maximum number of iterations limited to 2500. With these parameters, the algorithm did not converge in six of these 66 epochs. We also used values for the step-size parameter that ranged between 0.85 and 0.95, as this parameter should take values close to, but also smaller than, one [25]. However, these six cases did not converge either. Thus, the whole analysis could only be performed in 60 real MEG epochs.

1) Preprocessing in real MEG data

First, we estimated the optimal *m* value for the 60 MEG epochs. The average *m* value was 30.9 ± 6.0 ICs (mean ± SD). Considering these *m* values, the preprocessing stage estimated that the external noise represented the 9.99% ± 14.65% (mean ± SD) of the total recorded energy. Thus, the average energy due to the inner sources was supposed to be the 90.01%. As the preprocessing included a dimension reduction, only a part of all the energy due to the inner components was retained by the extracted ICs. It was estimated that the extracted ICs kept the 99.27% ± 0.47% (mean ± SD) of the total inner energy.

2) Artifact detection in real MEG data

Once we had preprocessed the epochs, we carried out the ICA decomposition. The estimated ICs were visually inspected in both time and frequency domains, and they were compared to the raw MEG data. By this procedure, we could classify the ICs into four groups: cardiac ICs, ocular ICs, line noise ICs, and other ICs (probably originated by the brain). In all epochs, one IC was responsible for the cardiac activity. In contrast, given the fact that MEG was recorded with eyes closed, only 21 of the 60 analyzed epochs had ocular artifacts. From these 21 MEG epochs, a total number of 36 ICs were due to ocular artifacts. Finally, 34 of the 60 MEG epochs showed line noise. In all of them, most power line noise was isolated into one IC.

KrE and *Skw* were calculated for each IC to detect the cardiac artifact. The IC that provided the maximum *KrE* or $\text{abs}(Skw)$ among all the ICs from the same MEG epoch might be due to the cardiac artifact. Our results showed that the *KrE* criterion was able to correctly recognize 49 of the 60 ICs (81.67%) that explained the cardiac signals. In most of the other 11 cases, *KrE* pointed to ocular ICs. On the other hand, *Skw* detected the cardiac artifact properly in 59 of the 60 cases (98.33%). Fig. 3 exemplifies the cardiac artifact recognition. We can observe that both ICs have leptokurtic amplitude distributions. In this case, the cardiac artifact has a lower *KrE* value (8.3735) than the other IC (9.5539). However, the larger $\text{abs}(Skw)$ was provided by the cardiac IC (2.2677 against 1.5442). To sum up, both ICs have leptokurtic amplitude distributions, which are easily detected by *KrE*. However, only *Skw* marks the cardiac artifact asymmetry.

Afterward, the proposed P_{LF} metric was used to recognize which ICs could be responsible for the ocular artifacts. In order to evaluate this metric, we analyzed the 36 ocular ICs and the 36 non-ocular-related ICs that had the largest fraction of their energy in the 0.5 Hz – 2.5 Hz band. Using the leave-one-out cross-validation ROC analysis, we found that the

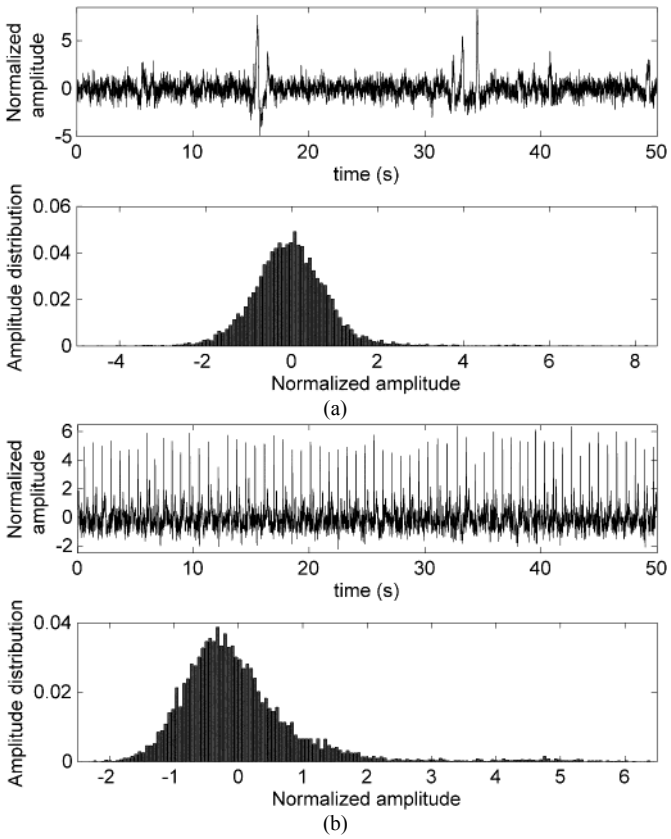

Fig. 3. Cardiac artifact detection by *KrE* and *Skw* on ICs from the same real MEG epoch. (a) IC wrongly marked as a cardiac artifact by *KrE* (*KrE* = 9.5539; *Skw* = 1.5442). (b) IC correctly marked as a cardiac artifact by *Skw* (*KrE* = 8.3735; *Skw* = 2.2677).

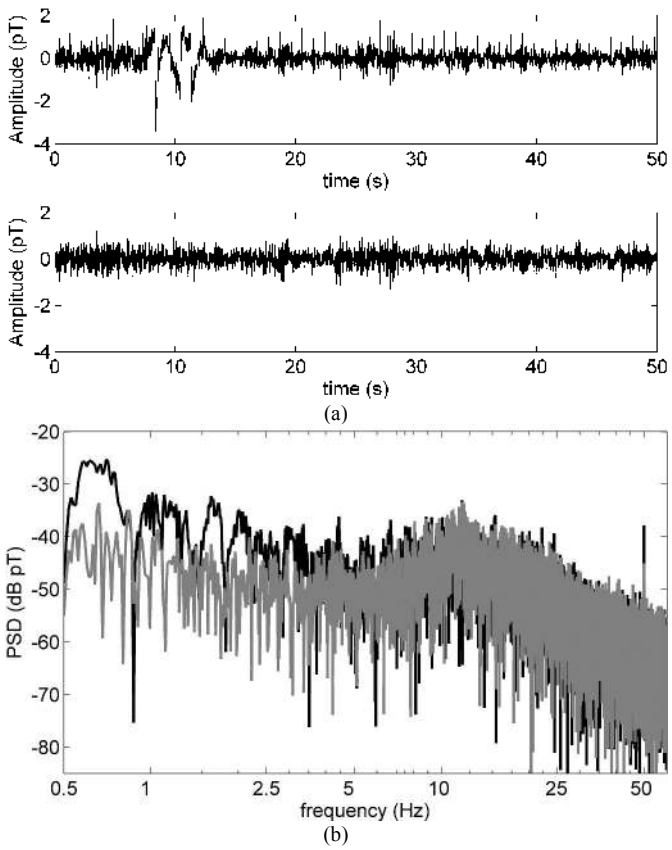

Fig. 4. Example of artifact removal in a real MEG epoch. (a) Time plot before (above) and after (below) artifact removal. (b) PSDs of the epoch before (black line) and after (grey line) artifact removal.

average optimum threshold th_{LF} = 0.3386 ± 0.0007 (mean ± SD) provided an accuracy of 86.11%. However, sensitivity (the fraction of ocular ICs correctly recognized) (97.22%) and specificity (the rate of non-ocular ICs properly detected) (75.00%) were very dissimilar. Therefore, we used the P_{EYES} metric to improve the classification rate for ocular artifacts, in order to avoid the nine false positives that P_{LF} had reported.

P_{EYES} was applied to the ICs that P_{LF} had previously marked as possible ocular artifacts. Thus, nine non-ocular and 35 ocular ICs were analyzed with the leave-one-out cross-validation ROC method to find the optimal th_{EYES} value, which was 0.1721 ± 0.0058 (mean ± SD). By linking both metrics, we achieved an accuracy of 94.44% in the ocular artifacts recognition: all the non-ocular ICs except one (specificity: 97.22%) and 33 of the 36 ocular ICs (sensitivity: 91.67%) were correctly classified. The incorrectly classified non-ocular IC had P_{LF} = 0.3763 and P_{EYES} = 0.1730.

In addition, we used the P_{50Hz} metric to assess the line noise in every IC. We could distinguish all main power line artifacts from the other ICs setting th_{50Hz} = 0.2326. Actually, the P_{50Hz} metric provided values larger than 0.4826 for all line noise ICs, whereas it offered values below th_{50Hz} for any other IC, irrespective of whether they came from MEG epochs with power line interference or not.

3) Artifact removal evaluation

First of all, Fig. 4(a) shows the example of a real MEG epoch severely contaminated by artifacts before and after BSS and artifact removal. The cardiac QRS-complexes are no longer visible. Moreover, Fig. 4(b) represents the corresponding PSDs. The brain activity spectrum has been enhanced over the ocular-related low frequencies.

Moreover, in order to assess the cardiac artifact removal, we detected QRS-waves in our data before and after the artifact rejection method using a template matching approach [27]. The mean QRS-waves are plotted in Fig. 5. The ICA-based artifact rejection has decreased the power of the QRS-waves considerably. Moreover, T-wave is no longer visible.

The ocular artifact removal was also evaluated computing the PSDs of the MEG epochs with ocular artifacts at the 13 channels included in the P_{EYES} metric before and after artifact removal. For comparison, the mean PSD of the MEG epochs that have no ocular artifacts was also computed at the same MEG channels. The low frequency ranges of these PSDs are depicted in Fig. 6. It can be seen that the low frequency energy of the ocular artifacts has been reduced.

Finally, the power line interference reduction was assessed similarly to how it was done in the ocular artifacts. The average PSD of the MEG epochs with power line noise was calculated before and after artifact removal at all channels. The mean spectra represented in Fig. 7 show that this artifact was attenuated around 17 dB.

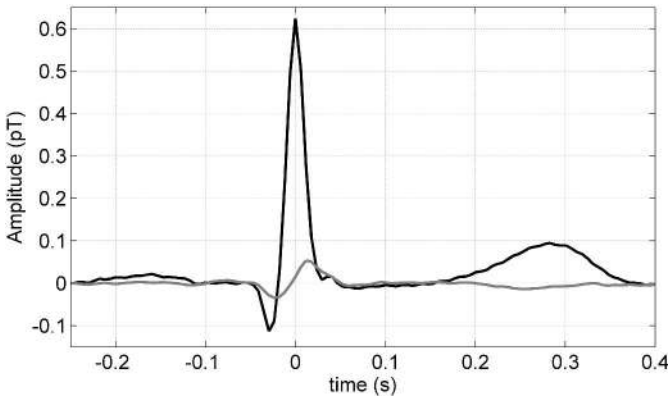

Fig. 5. Average QRS-complex of the cardiac artifact that appears in MEG data before (black line) and after (grey line) artifact rejection.

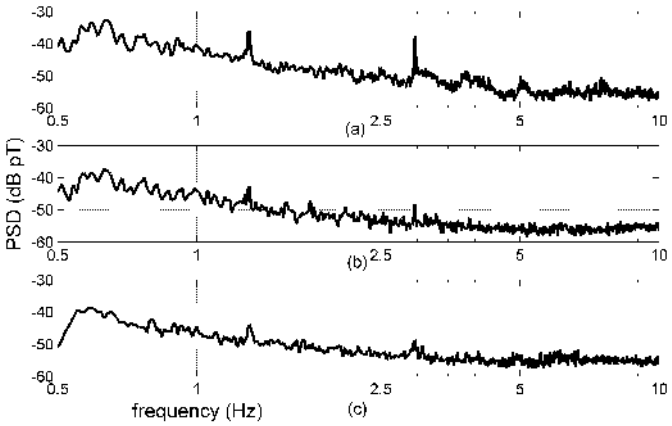

Fig. 6. Mean PSDs of the MEG epochs contaminated by ocular artifacts at the channels considered in the P_{EYES} metric before (a) and after (b) artifact removal. For comparison, the mean PSD of the MEG epochs without ocular artifacts at the same MEG channels is also shown after artifact removal (c).

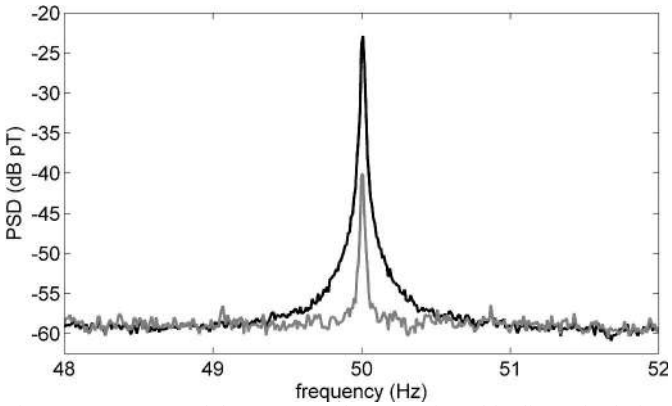

Fig. 7. Mean PSDs of the MEG epochs contaminated by line noise before (black line) and after (grey line) artifact removal.

IV. Discussion and Conclusions

In order to detect and remove line noise, cardiac, and ocular artifacts from MEG data, we have used an ICA-based method. This method consists of three stages:

1) A robust preprocessing [23] and a statistical criterion [22] to decide the value of *m*.
2) A robust ICA algorithm [25] to estimate the ICs.
3) Several metrics to detect the aforementioned artifacts once they have been isolated from brain activity.

MEG data usually have redundant information at adjacent SQUIDs [2]. In addition, the main assumption made by ICA is that brain activity and artifacts are mutually independent [2]. Consequently, ICA may allow us to isolate artifacts preserving the integrity of the brain activity.

The whole method was tested on simulated data. The estimations of the additive noise power and the number of ICs were satisfactory for average channel SNRs larger than 3 dB. Moreover, the *MDL* metric estimated *m* more accurately than the PCA-subspace approaches [16], which are rather arbitrary and may produce results that depend on the shape of the eigenvalue spectrum [2]. In contrast, both problems are avoided with the technique used in this study. In addition, the detection of the artifacts simulated in synthetic data suggested that the proposed method could be useful for real MEG data.

Before the CII algorithm was applied to real data, we preprocessed the MEGs to reduce their dimensionality and to avoid overfitting problems [2]. The *MDL* metric [22] selected the *m* value for every MEG epoch automatically. From the 148 available MEG channels, the mean estimated number of ICs was 30.9 ± 6.0 (mean ± SD). With these *m* values, the averaged energy retained was 99.27% ± 0.47% (mean ± SD).

Some work has dealt with the cardiac artifact rejection in MEG data. In [18], the cardiac and ocular artifacts were marked by kurtosis and entropy due to their amplitude distributions. Moreover, the artifact recognition could be improved by computing the correlation between each IC and reference ECG and EOG signals. However, neither kurtosis nor entropy marked only one of these kinds of artifacts, and few MEG epochs were analyzed [18]. In [15], the cardiac artifact subspace was recognized in MEG data by studying its field map, time series, and power spectrum. In contrast, we found that *Skw* outperformed kurtosis in the cardiac artifact detection: *Skw* detected ten artifacts that *KrE* had missed. The reason is that, whereas *KrE* offers high values for leptokurtic amplitude distributions (i.e., ocular and cardiac ICs), *Skw* marks asymmetrical distributions, which are more typical of cardiac artifacts. In all analyzed MEG epochs, the cardiac activity was mainly isolated into only one IC. This might be due to the differences between the amplitude distribution of a typical cardiac artifact and those of other ICs. However, if there were more than one cardiac IC, our metric would only detect at most one of them.

Several studies have developed methods to remove ocular artifacts from EEGs [16], [20], [21] and MEGs [18] with BSS. Some of them are based on the ocular scalp pattern [21] or on the correlation with an EOG reference signal [18], [20]. Our approach is different. We linked two straightforward metrics that do not use any EOG reference channel. First, we found the ICs that had most of their power in low frequencies (0.5 Hz to 2.5 Hz). Then, we applied a criterion focused on the detection of which previously marked ICs had a relevant fraction of their power near the eyes. We found that, by joining both criteria, the results were improved in relation to the accuracy achieved

using only one of them. The leave-one-out cross-validation analysis revealed a non-ocular-related IC that was classified as an ocular artifact. This kind of errors should be minimized, as possibly useful brain activity may be removed. The P_{LF} and P_{EYES} values for this false artifactual IC were close to the th_{LF} and th_{EYES} values. This suggests that this false positive may be avoided by a small increase of the th_{LF} and/or th_{EYES} values, although the sensitivity of the artifact detection may decrease.

The typical method to avoid line noise is to filter it in the frequency domain. However, when the line frequency overlaps the analyzed frequency band, some other approach may be needed [11]. To detect the ICs that accounted for the main power line interferences, we calculated the fraction of the PSD centered at 50 Hz. Marking as line noise artifacts the ICs with P_{50Hz} values larger than a threshold, we could clearly detect all major power line ICs without removing brain activity.

In the BSS-based artifact rejection, the brain signals without artifacts are unknown. Therefore, assessing the artifact removal is not straightforward because the separation cannot be absolutely validated [2], [18]. However, the processed brain signals may be compared with the raw recordings to estimate how much artifactual activity has been removed.

In order to assess the cardiac artifact rejection, we located and averaged the QRS-complexes which appeared in MEG data before artifact removal [27]. Then, we compared them with the mean of the corresponding pieces of signal after artifact rejection. We found that the T-wave had been removed and the QRS-complex power had decreased significantly. The residual QRS-waves may be due to the fact that some extracted ICs could have small remainders of the cardiac artifact hidden by much stronger brain activity. In addition, Fig. 6 allowed us to assess the ocular artifact rejection. It can be seen that the low frequency energy related to the ocular activity has been removed from the signals. Finally, we could reduce line noise without removing brain activity. However, this artifact was not entirely rejected. The mean attenuation was about 17 dB. A previous study reported that ICA could isolate around 75% of line noise into one IC applying the extended infomax algorithm [9] to EEGs heavily contaminated by line noise at 60 Hz [11]. The dissimilar ability of both approaches to reject this artifact might be due to the different ICA algorithms applied or to the number of estimated ICs.

Our study has some limitations that merit consideration. Firstly, the sample size was small, and further analysis must be carried out with a larger number of epochs. Moreover, the use of different MEG recording equipment may influence the proposed artifact detection metrics. Secondly, we used a closed-eyes, background activity recording paradigm. This allowed us to minimize blinks and fast eye movements, but the alpha wave may rise. Moreover, the lack of a visual reference may increase low-frequency eye movements [6]. This might be useful to discern ocular ICs from brain activity, as the ocular artifacts may shift toward lower frequencies. However, our results may not be directly generalized to other settings where open-eyes recordings are needed. Moreover, brain activity might have a 1/f spectrum and be focused in frontal areas. Hence, if the subject's brain activity had these characteristics, it might interfere with the ocular artifact recognition method. Therefore, more tests with larger and different databases are needed to further assess the performance of our method. Finally, the CII algorithm could not decompose six of the 66 MEG epochs. Although this lack of convergence limits our study, we considered that the 60 MEG epochs which could be decomposed were a large enough representative sample of the database. However, further studies with other robust BSS algorithms should be carried out to decompose those six epochs and to assess whether the artifact detection criteria depend on the BSS algorithm.

In summary, our analysis suggests that the proposed criteria could be useful to detect line noise, cardiac, and ocular artifacts after ICA has been applied to the MEGs. We found that *Skw* detected 59 of the 60 ICs (98.33%) related to cardiac artifacts, whereas *KrE* only marked 49 of them (81.67%). In addition, linking a power threshold on the PSD of the ICs and a criterion on their scalp field, we could identify correctly 33 of the 36 ocular (91.67%) and all the non-ocular ICs except one (97.22%). Moreover, the line noise ICs could be rejected by a metric based on the fraction of the PSD at 50 Hz. Finally, the comparison of the MEG signals before and after artifact removal showed that the proposed methods considerably reduced the power of the cardiac and ocular artifacts. Furthermore, although line noise was still present in MEG data after artifact removal, it had been attenuated about 17 dB.

ACKNOWLEDGMENT

The authors are thankful for the useful feedback of the Reviewers on the manuscript.

REFERENCES

[1] R. Hari, "Magnetoencephalography in clinical neurophysiological assessment of human cortical functions," in *Electroencephalography: Basic Principles, Clinical Applications, and Related Fields*, 5th ed., E. Niedermeyer, and F. Lopes da Silva, Ed. Philadelphia: Lippincott Williams & Wilkins, 2005, pp. 1165–1197.

[2] C. J. James and C. W. Hesse, "Independent component analysis for biomedical signals," *Physiol. Meas.*, vol. 26, no. 1, pp. R15–R39, Feb. 2005.

[3] V. Jousmäki and R. Hari, "Cardiac artifacts in magnetoencephalogram," *J. Clin. Neurophysiol.*, vol. 13, no. 2, pp. 172–176, Mar. 1996.

[4] A. Antervo, R. Hari, T. Katila, T. Ryhänen, and M. Seppänen, "Magnetic fields produced by eye blinking," *Electroenceph. Clin. Neurophysiol.*, vol. 61, no. 4, pp. 247–253, Oct. 1985.

[5] S. Vorobyov and A. Cichocki, "Blind noise reduction for multisensory signals using ICA and subspace filtering, with application to EEG analysis," *Biol. Cybern.*, vol. 86, no. 4, pp. 293–303, Apr. 2002.

[6] R. J. Croft and R. J. Barry, "Removal of ocular artifact from the EEG: a review," *Neurophysiol. Clin.*, vol. 30, no. 1, pp. 5–19, Feb. 2000.

[7] P. K. Sadasivan and D. N. Dutt, "SVD based technique for noise reduction in electroencephalographic signals," *Signal Process.*, vol. 55, no. 2, pp. 179–189, Dec. 1996.

[8] P. Comon, "Independent component analysis – A new concept?," *Signal Process.*, vol. 36, no. 3, pp. 287–314, Apr. 1994.

[9] A. Hyvärinen, J. Karhunen, and E. Oja, *Independent component analysis*. New York: Wiley, 2001.

[10] R. Vigário and E. Oja, "Independence: a new criterion for the analysis of the electromagnetic fields in the global brain?," *Neural Netw.*, vol. 13, no. 8, pp. 891–907, Oct.-Nov. 2000.
[11] T. P. Jung, S. Makeig, C. Humphries, T. W. Lee, M. J. McKeown, V. Iragui, and T. J. Sejnowski, "Removing electroencephalographic artifacts by blind source separation," *Psycophysiol.*, vol. 37, no. 2, pp. 163–178, Mar. 2000.
[12] R. Reyment and K. G. Jöreskog, *Applied factor analysis in the natural sciences*. Cambridge: Cambridge University Press, 1993.
[13] C. Jutten and J. Herault, "Blind separation of sources, Part I: an adaptive algorithm based on neuromimetic architecture," *Signal Process.*, vol. 24, no. 1, pp. 1–10, Jul. 1991.
[14] R. N. Vigário, "Extraction of ocular artefacts from EEG using independent component analysis," *Electroenceph. Clin. Neurophysiol.*, vol. 103, no. 3, pp. 395–404, Sep. 1997.
[15] T. H. Sander, G. Wübbeler, A. Lueschow, G. Curio, and L. Trahms, "Cardiac artifact subspace identification and elimination in cognitive MEG data using time-delayed decorrelation," *IEEE Trans. Biomed. Eng.*, vol. 49, no. 4, pp. 345–354, Apr. 2002.
[16] K. H. Ting, P. C. W. Fung, C. Q. Chang, and F. H. Y. Chan, "Automatic correction of artifact from single-trial event-related potentials by blind source separation using second order statistics only," *Med. Eng. Phys.*, vol. 28, no. 8, pp. 780–794, Oct. 2006.
[17] A. Delorme, S. Makeig, and T. Sejnowski, "Automatic artifact rejection for EEG data using high-order statistics and independent component analysis," in *Proc. 3rd International Workshop on ICA*, San Diego, 2001, pp. 457–462.
[18] G. Barbati, C. Porcaro, F. Zappasodi, P. M. Rossini, and F. Tecchio, "Optimization of an independent component analysis approach for artifact identification and removal in magnetoencephalographic signals," *Clin. Neurophysiol.*, vol. 115, no. 5, pp. 1220–1232, May 2004.
[19] C. J. James and O. J. Gibson, "Temporally constrained ICA: an application to artifact rejection in electromagnetic brain signal analysis," *IEEE Trans. Biomed. Eng.*, vol. 50, no. 9, pp. 1108–1116, Sep. 2003.
[20] C. A. Joyce, I. F. Gorodnitsky, and M. Kutas, "Automatic removal of eye movement and blink artifacts from EEG data using blind component separation," *Psycophysiol.*, vol. 41, no. 2, pp. 313–325, Mar. 2004.
[21] Y. Li, Z. Ma, W. Lu, and Y. Li, "Automatic removal of the eye blink artifact from EEG using an ICA-based template matching approach," *Physiol. Meas.*, vol. 27, no. 4, pp. 425–436, Apr. 2006.
[22] S. Ikeda and K. Toyama, "Independent component analysis for noisy data – MEG data analysis," *Neural Netw.*, vol. 13, no. 10, pp. 1063–1074, Dec. 2000.
[23] J. Cao, N. Murata, S. Amari, A. Cichocki, and T. Takeda, "A robust approach to independent component analysis of signals with high-level noise measurements," *IEEE Trans. Neural Netw.*, vol. 14, no. 3, pp. 631–645, May 2003.
[24] R. Vigário, J. Särela, V. Jousmäki, M. Hämäläinen, and E. Oja, "Independent component approach to the analysis of EEG and MEG recordings," *IEEE Trans. Biomed. Eng.*, vol. 47, no. 5, pp. 589–593, May 2000.
[25] S. Cruces, L. Castedo, and A. Cichocki, "Robust blind source separation algorithms using cumulants," *Neurocomputing*, vol. 49, no. 1, pp. 87–118, Dec. 2002.
[26] M. H. Zweig and G. Campbell, "Receiver-Operating Characteristic (ROC) plots: a fundamental evaluation tool in clinical medicine," *Clin. Chem.*, vol. 39, no. 4, pp. 561–577, Apr. 1993.
[27] M. Samonas, M. Petrou, and A. A. Ioannides, "Identification and elimination of cardiac contribution in single-trial magnetoencephalographic signals," *IEEE Trans. Biomed. Eng.*, vol. 44, no. 5, pp. 386–393, May 1997.